# Under–expanded jet noise prediction using surrogate models based on artificial neural networks

Francesco Centracchio * Stefano Meloni [†],
*Roma Tre University, Department of Engineering, Via Vito Volterra, 62, 00146 Rome (Italy)*

Hasan Kamliya Jawahar [‡] Mahdi Azarpeyvand [§]
*University of Bristol, Bristol, United Kingdom, BS8 1TR*

Roberto Camussi [¶] and Umberto Iemma [‖]
*Roma Tre University, Department of Engineering, Via Vito Volterra, 62, 00146 Rome (Italy)*

**The use of surrogate models in recent times plays a key role in the design process and, over the past few years, machine learning algorithms are adapting to the use of active metamodelling techniques. In the present study, Artificial Neural Networks formulation is used as a data–driven nonlinear model aimed at describing the dynamics of an experimental test campaign related to the noise emitted by a single–stream jet in under–expanded conditions. The architecture of the neural network is selected employing a deterministic optimization algorithm, coupled with data informed tuning of the input parameters. The data set explored here was acquired in the state–of–the–art aeroacoustic facility at the University of Bristol. Both the near- and far–field acoustic measurements were carried out for a cold under–expanded jet for Mach numbers ranging from 1.1 to 1.4. The predictions by the metamodel are in good agreement with the experimental data, and the results demonstrate the capability of metamodels as a reliable tool to estimate jet noise in under-expanded flow conditions for a wide range of Mach numbers and near–field locations.**

## I. Introduction

This works presents a data–driven surrogate model based on Artificial Neural Networks (ANN) for the prediction of the near–field noise generated by a cold jet in under–expanded conditions. The relevant framework is the use of suitable noise prediction tools within the so–called Simulation Based Design (SBD) for aircraft. Over the past few years, the use of SBD in many engineering fields [1] has led the researchers towards increased use of metamodels to describe the dynamics of simulations or experimental data: such an approach considerably reduces the effort of the designers, ensuring a more reliable knowledge of the design space. To date, a large number of metamodelling strategies are used [2–4] to support the design process, and surrogate models built through ANN are starting to gain increasing relevance. Although the formalization of the input–output relations of the artificial neurons dates back to the 40s [5, 6], the increase in computing resources within the last 50 years [7–10] led to the exploration of complex multilayer structures, which ensure the capability to easily address many engineering problems such as computer vision and speech recognition [11]. More recently, models built using ANN are also being successfully exploited in the field of aeroacoustics [12–14], along with the well–assessed Radial Basis Functions (RBF) technique [15].

The ANN metamodel is here exploited as data–driven model with the aim at representing a dataset built starting from aeroacoustic measurements of a cold jet. The relevance of the physical problem presented in this work lies in the fact that during the cruise phase, due to the combined effect of low external static pressure and required thrust to maintain the flight Mach number, the jet exhausting flow is under–expanded [16, 17]. This nozzle condition generates a jet plume with a complex flow pattern characterized by a series of oblique compression and expansion waves that form the so–called shock–cell sequence [18]. The presence of these complex flow structures introduces further sound

*PhD, Department of Engineering, francesco.centracchio@uniroma3.it
[†]Research Fellow, Department of Engineering, stefano.meloni@uniroma3.it
[‡]Research Associate, Department of Aerospace Engineering, hasan.kj@bristol.ac.uk
[§]Professor, Department of Mechanical Aerospace, m.azarpeyvand@bristol.ac.uk
[¶]Professor, Department of Engineering, roberto.camussi@uniroma3.it
[‖]Professor, Department of Engineering, umberto.iemma@uniroma3.it

generation mechanisms, likes Broadband Shock Associated noise (BBSAN) and Screech tones that are in addition to the turbulent jet mixing noise also present in the subsonic case. The BBSAN was first identified by Harper-Bourne and Fisher [19], and it is generated from a weak interaction between downstream propagating large turbulent structures and the quasi–periodic shock cells in the jet plume. This is the dominant noise component for an under–expanded jet in the upstream direction. Screech is a form of aeroacoustic resonance present in shock–containing under–expanded jets: it was first identified by Powell [20], which defined the feedback loop as generated by a disturbance that propagates downstream from the nozzle lip, interacts with the shock–cells, and comes back upstream, closing the resonant loop at the nozzle lip. Observations reveal that when a jet emits strong screech tones, the flow has strong oscillations characterized by different modes [21–23] (*e.g.* helical, toroidal, and flapping modes).

For the first time we present a data–driven ANN–based metamodel capable of predicting the jet noise spectra of the near–field noise emitted by a jet in under–expanded conditions. The database used to train the model contains time–resolved signals acquired in the BJARF aeroacoustic facility at the University of Bristol. The measurements were made using a near-field microphone array positioned at different radial distances from the jet axis between h/D=1.5 and h/D=10.5. The array comprises ten microphones located in the stream–wise direction between x/D=0 and x/D=18. Far-field measurements considered for the model were acquired using a polar array positioned at 1.6m from the jet axis.

The choice of ANN architecture is a crucial task for designers since the network hyperparameters affect model response throughout the domain. Indeed, the ANN fitting capability is known to be sensitive to the network architecture, and the set of topologies capable to correctly fit the training data is strongly problem dependent. Unfortunately, there is not a specific scheme to find the optimal or near–optimal configuration of hidden layers, thus a recently–implemented in–house architecture optimiser has been used to derive the ANN model architecture. The optimiser automatically selects both the number of hidden layers and nodes, together with the best combination of activation functions: the algorithm is coupled with a self–tuning scheme for the automatic selection of learning rate and batch size. The self–tuning algorithm has demonstrated to be accurate and efficient, as well as the architecture optimiser and the observed performance discloses the possibility to implement numerical strategies for the reliable and robust design in aeronautics. It is worth highlighting that, since the ANN model can predict function values in regions of the domain where there are no experiments, an uncertainty function must be provided to estimate the reliability of the model itself. Here, the ANN response is assumed to be the expectation of a posterior stochastic process, and the spatial correlation is used to derive the uncertainty function on the whole domain.

The work is organized as follows. The active ANN metamodel formulation is detailed in Sec. II, with special attention paid to the definition of the uncertainty function. An overview of the experimental setup is in Sec. III, whereas the numerical results are presented and discussed in Sec. IV. Sec. V gathers the conclusions outlining the future work.

## II. Active metamodelling with Neural Networks

The ANN metamodel is aimed at representing the fundamental dynamics of a physical phenomenon through an analytical function, starting from a limited knowledge of the actual output obtained via simulations or experiments. At first let us consider a multilayer dense structure (composed by one or more intermediate hidden layers, each consisting of one or more neurons, in addition to the input and the output layers): the output of each layer can be written as it follows

$$\mathbf{a}_l = \boldsymbol{\phi}_l \left( \mathbf{W}_{l\text{-}1} \mathbf{a}_{l\text{-}1} + \mathbf{b}_l \right), \quad l = 2, \ldots, L \tag{1}$$

so that the inputs $\mathbf{x} \equiv \mathbf{a}_1$ and the outputs $\mathbf{y} \equiv \mathbf{a}_L$. In the Eq. (1) the term $\boldsymbol{\phi}_l$ is the vector containing the activation functions of the $l$-th layer, $\mathbf{W}_{l\text{-}1}$ is the matrix of the weights, and $\mathbf{b}_l$ the vector containing the bias values: the well–known *backpropagation* method is used to compute the unknown weights matrices and biases vectors of Eq. (1). This technique basically consists of the minimisation of the following cost function

$$C_t = \frac{1}{2} \sum_{i=1}^{R} \left( \mathbf{d}_i - \mathbf{y}_{i,t} \right)^2 \tag{2}$$

for a prescribed number of epochs $T$: in Eq. (2) $R$ is the number of training set patterns, $\mathbf{d}_i$ is the output vector and $\mathbf{y}_{i,t}$ the network output at the $t$-th epoch, both related to the $i$-th training pattern. The gradient of the cost function $C_t$ is computed as a series of local intermediate components obtained by backpropagating the information flow from the output layer down to the input one: downstream the backpropagation, weights and biases are updated by means of the learning rate $\eta$. Once the training process is complete, the network can be identified by its parameters $\Theta = \{\mathbf{f}_l, \mathbf{W}_{l\text{-}1}, \mathbf{b}_l\}_{l=2}^{L}$, and the the network output is such that $\hat{\mathbf{y}}_\mathbf{i}$ is the image of $\mathbf{x}_i$. A schematic representation of a neural network is in Fig. 1.

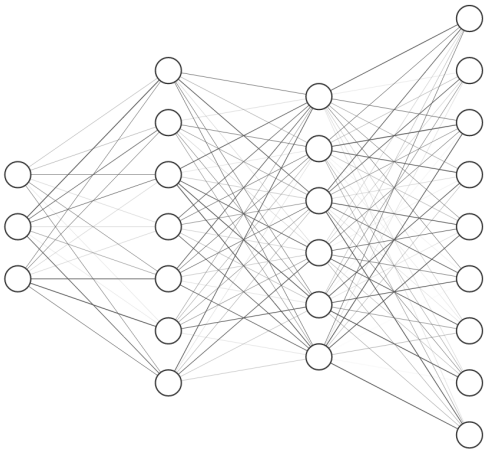

**Fig. 1 Schematic representation of a neural network with 3 input nodes, two hidden layers (with 7 and 6 nodes respectively) and 9 output nodes.**

It is known that there is no specific rule to find the optimal or near–optimal network configuration in terms of activation functions and topology: here, a recently implemented fully–deterministic optimization scheme has been used to derive the metamodel architecture. The initialization of weights and biases is performed using uniform random deviate distributions of numbers between 0.0 and 1.0, generated with a fixed seed: afterward, the Box–Muller transform is applied to make the distributions normally distributed with zero expectation and unit variance. Activation functions and batch size are chosen after a preliminary tournament. The number of layers and neurons per layer is selected through a minimization problem, which accounts for the Root Mean Square Error (RMSE), related to both the training set and the validation set. The network training is facilitated by a dynamic update of the learning rate $\eta$, to mitigate the effects of the learning instabilities. An early stopping criterion determines whether or not to continue the training of the current network configuration [14].

Since the metamodel aims at predicting the functions in the whole domain, even in regions where there are no true values, the definition of a merit function representing the behaviour of the metamodel uncertainty plays a key role. By definition, the uncertainty must equals zero at the training points, as the prediction accuracy set by the designer is ensured by current optimal topology. Here, the uncertainty function is supposed to be linked to the spatial correlation: specifically, the standard deviation $\sigma_{\mathcal{N}}(\mathbf{x})$ related to the posterior stochastic process is modelled as it follows

$$\sigma_{\mathcal{N}}(\mathbf{x}) = \begin{cases} \left[ \dfrac{\sum_{j=1}^{N} \omega_j(\mathbf{x}) \hat{y}_j}{\sum_{j=1}^{N} \omega_j(\mathbf{x})} - \hat{y}(\mathbf{x}) \right]^2 & \text{if} \quad \Delta_j(\mathbf{x}) \neq 0 \quad \forall j \\ 0 & \text{if} \quad \exists j | \Delta_j(\mathbf{x}) = 0 \end{cases} \tag{3}$$

being $\omega_j(\mathbf{x}) = \Delta_j^{-\alpha}$ with $\Delta = d(\mathbf{x}, \mathbf{x}_j)$ the Euclidean distance of a generic point $\mathbf{x} \in \mathcal{D}$ and $\mathbf{x}_i \in \mathcal{T}$, with $\mathbf{x}$ the generic domain point. The parameter $\alpha$ of Eq. (3) controls the decay law of the influence of distant points. Under the hypothesis of a continuous uniform distribution with expectation $\hat{y}$ (the network predictions) and variance $\sigma^2_{\mathcal{N}}(\mathbf{x})$, the global uncertainty $U(\mathbf{x})$ can be computed as it follows

$$U(\mathbf{x}) = \sqrt{\frac{1}{N} \sum_{j=1}^{N} u_j^2(\mathbf{x})} \tag{4}$$

being $u_j(\mathbf{x}) = 2\sqrt{3}\sigma_{\mathcal{N}}(\mathbf{x})$ the uncertainty related to each component of the vector function. The relevance of the uncertainty function also lies on the possibility to identify the regions of the domain where knowledge of the data should be improved with additional experiments. Indeed, a new training point can be selected as it follows

$$\mathbf{x}_{new} = \arg\max_{\mathbf{x} \in \mathcal{D}} [U(\mathbf{x})] \tag{5}$$

so that the size of the training set is increased, and a new network can be built using the active scheme described above.

## III. Experimental setup

The experiments were conducted at the new jet aeroacoustic facility (BJARF) at the University of Bristol. The jet flow in the facility is conditioned and silenced using three different in–line–silencers to create a quiet flow. The first two silencers were placed right after the control valve outside the anechoic chamber and has a diameter of 0.3 m and a height of 1.5 m each. The third large silencer was placed inside the chamber and has a diameter of 0.457 m and a height of 1.9 m. The silencers were equipped with perforated tubes for the flow with the remaining area packed with glass wool. The anechoic chamber has dimensions of 7.9 m in length, 5.0 m in width and 4.6 m in height, including the surrounding acoustic walls and a cut-off frequency of 160Hz [24, 25].

In this application the jet flow exhausts from a convergent contoured nozzle having an exit diameter of 16.993mm, and has been obtained by 3:1 down-scaling the SMC000 nozzle proposed by [26]

The tests were carried out for a wide range of subsonic flows with Mach number $M$ ranging from 1.1 up to 1.4, by step of M=0.1. Near–field noise measurements were performed using 1/4–inch G.R.A.S 40PL microphones for $t = 12$ s and at a sampling frequency of $f = 2^{17}$Hz. As shown in Fig. 2, the near–field measurements were carried with a linear array of 10 microphones placed at a distance of 2D away from each other, moved to 12 different heights $h$ radially away from the jet centre–line using an high precision traversing system. The closest height was chosen to be $h = 1.5D$ to avoid grazing of flow on the microphone and the last one is at $h = 10.5D$. Far-field measurements were carried out using an array of 18 microphones distributed on an arc centred on the jet exit at a distance of 1.6 m ($\approx 95D$) that covered an angle between 60° upstream and 155° downstream with the 90° microphone positioned right above the nozzle exit (see Fig. 2).

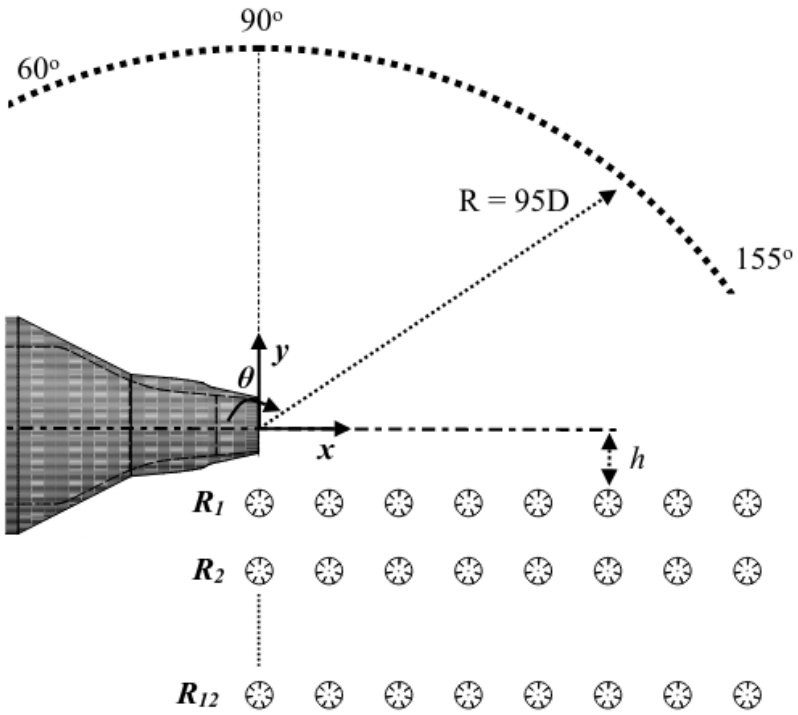


**Fig. 2 Sketch of the experimental setup.**

To the extent of the noise level estimations, the sound pressure level, (SPL) was calculated using SPL formulation reported as reported in the following equation:

$$SPL = 10\log_{10}\left(\frac{\mathrm{PSD}\Delta f_{\mathrm{ref}}}{P_{\mathrm{ref}}^2}\right), \tag{6}$$

where PSD denotes the power spectral density evaluated using Welch's method, $\Delta f_{\mathrm{ref}}$ is the frequency bandwidth and $P_{\mathrm{ref}}$ is the reference pressure in air (equal to $20\mu$Pa).

Spectra have been represented in $1/3$–octave bands: the rationale underlying this choice lies in the fact that most aircraft noise prediction tools widely used in the aircraft design process make use of the $1/3$–octave bands description of the pressure signals from 50 Hz up to 10 kHz, as required by regulations. In addition, using the bands representation considerably reduces the number of training set data, resulting in faster network training.

## IV. Results and discussion

The data of the experimental campaign were used to create a database consisting of 160 elements, each one composed by the 3 independent variables with associated the 28 components of the SPL spectrum (related to the centre frequencies in $1/3$–octave bands). The dataset has been randomly shuffled, thus 140 elements were used as training set $\mathcal{T}$ whereas 20 as validation set $\mathcal{V}$. In this view, the vector collecting the $1/3$–octave bands SPL is a function of $x/D$, $h/D$ and $M$: this implies 3 input neurons and 28 output neurons.

For the architecture optimization the maximum number of hidden layers has been set equal to 3, and several activation functions have been used for the tournament (gaussian, sigmoid, hyperbolic tangent, swish, identity, hyperbolic secant and cardinal sine). The stop criterion was based on the normalised RMSE on the training set points $\text{RMSE}_{\mathcal{T}}$, whereas the validation error $\text{RMSE}_{\mathcal{V}}$ was analysed in runtime during the training to prevent the overfitting, stopping the training of the current configuration. The $\text{RMSE}_{\mathcal{T}}$ target accuracy was set equal to 1%, and the optimization algorithm reached the convergence value in 404 iterations, as shown in Fig. 3.

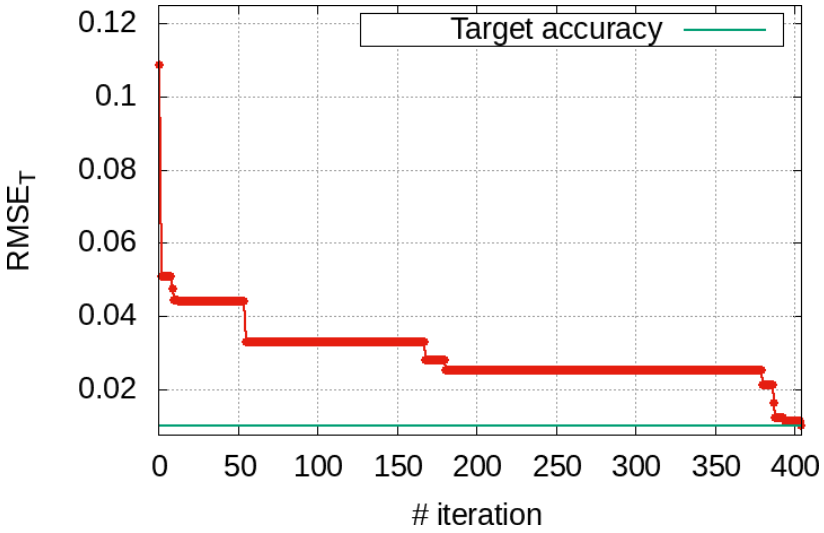


**Fig. 3 $\text{RMSE}_{\mathcal{T}}$ as a function of the number of iterations.**

The optimised network architecture obtained by means of the minimisation process has the characteristics reported in the table Tab. 1.

**Table 1 ANN metamodel final configuration.**

| | |
|---|---|
| Final topology | 3/27/40/28 |
| Hidden layer activation | *gaussian* |
| Output layer activation | *sigmoid* |
| $\text{RMSE}_{\mathcal{T}}$ | 0.99% |
| $\text{RMSE}_{\mathcal{V}}$ | ~3.0% |

Since the initial requirement of a model is its ability to reproduce the data, let analyse the network response in some points belonging to the training set: this capability has paramount relevance in handling large databases, as allows the designers to completely replace the dataset with a small number of network hyperparameters that describe the dynamics of the data. Figure 4 show the comparison between model and data in known points.

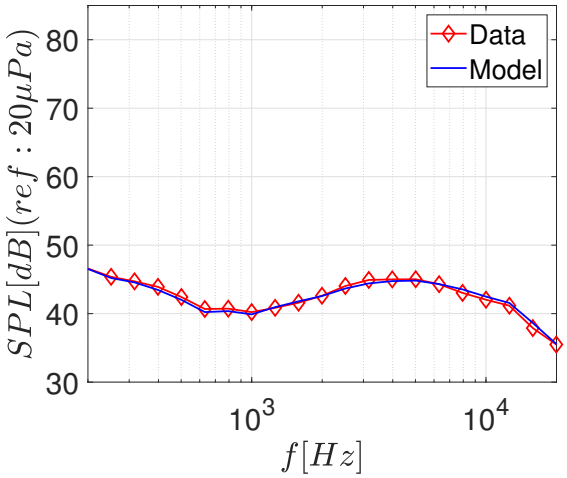


(a) SPL data and model for $M = 1.1$, $x/D = 18$ and $h/D = 10.5$

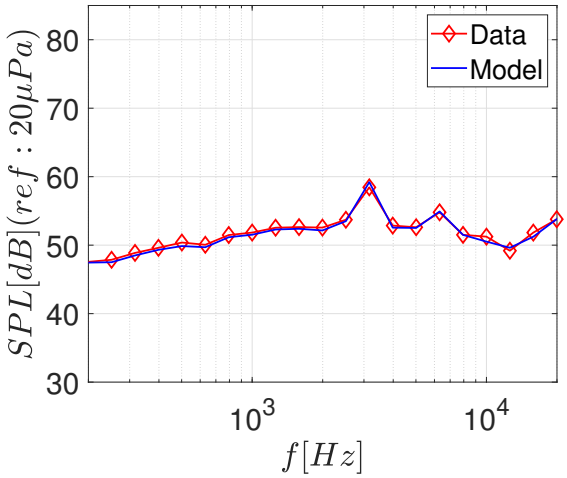


(b) SPL data and model for $M = 1.2$, $x/D = 4$ and $h/D = 3.5$

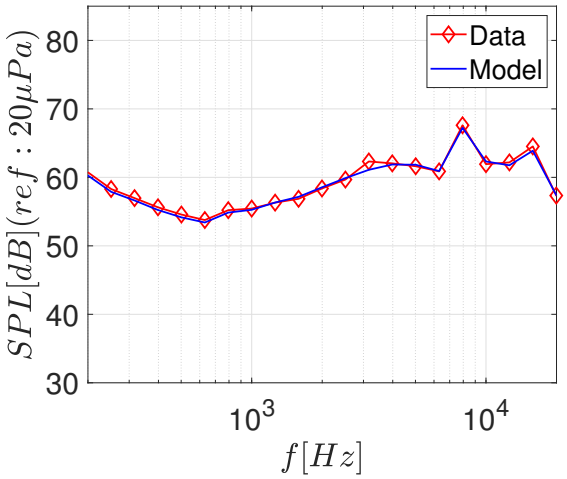


(c) SPL data and model for $M = 1.3$, $x/D = 6$ and $h/D = 1.5$

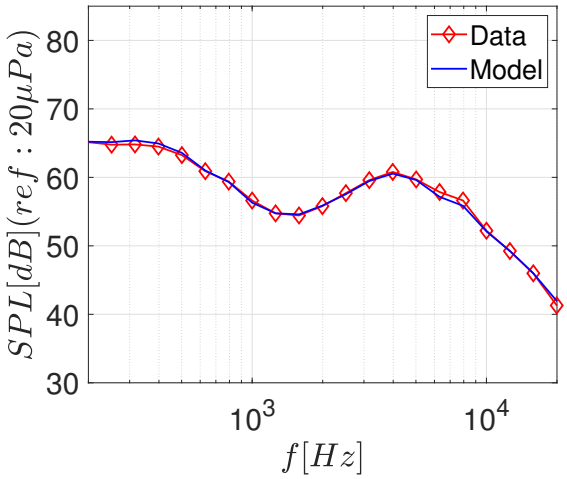


(d) SPL data and model for $M = 1.3$, $x/D = 18$ and $h/D = 5.5$

**Fig. 4 Comparison between ANN metamodel response and original data at different known locations.**

The analysis of Fig. 4 highlights that the ANN model is in excellent agreement with the experimental data: the network is fully capable to reproduce the broadband noise, as well as the the 1/3-octave bands representation of the tonal components (see Figs. 4b and 4c). It can easily be noted that the selected target $\text{RMSE}_{\mathcal{T}}$ accuracy (set equal to 1% over the points belonging to the training set $\mathcal{T}$) guarantees an absolute error always lower than 0.25 dB, which fully satisfies the requirements of a predictive noise model. The model $\text{RMSE}_{\mathcal{T}}$ turns out to be lower than $\sim 3\%$ (see Tab. 1) over the whole domain of interest, ensuring the absence of overfitting within the limits of applicability.

A metamodel is also capable of making predictions within the entire domain (it can be shown that extrapolation of data outside the domain, as far as theoretically possible, is definitely to be avoided): in this way it is possible to make a forecast of the phenomenon where there are no experimental data. Thus, let analyse the model behaviour in a not measured point: Fig. 5 shows the model response at $h/D = 3.5$ and $x/D = 3.5$ (for all the Mach numbers between 1.1 and 1.4), with associated the uncertainty values.

Results in Fig. 5 are consistent with the literature and the physics. Despite the bands representation, the Screech tone is clearly visible in Fig. 5a: as expected, it appears at $M > 1.15$ and the maximum amplitude increases with $M$. The frequency of the Screech tone is almost constant with $M$, showing a slight drop in frequency starting from $M \approx 1.32$.

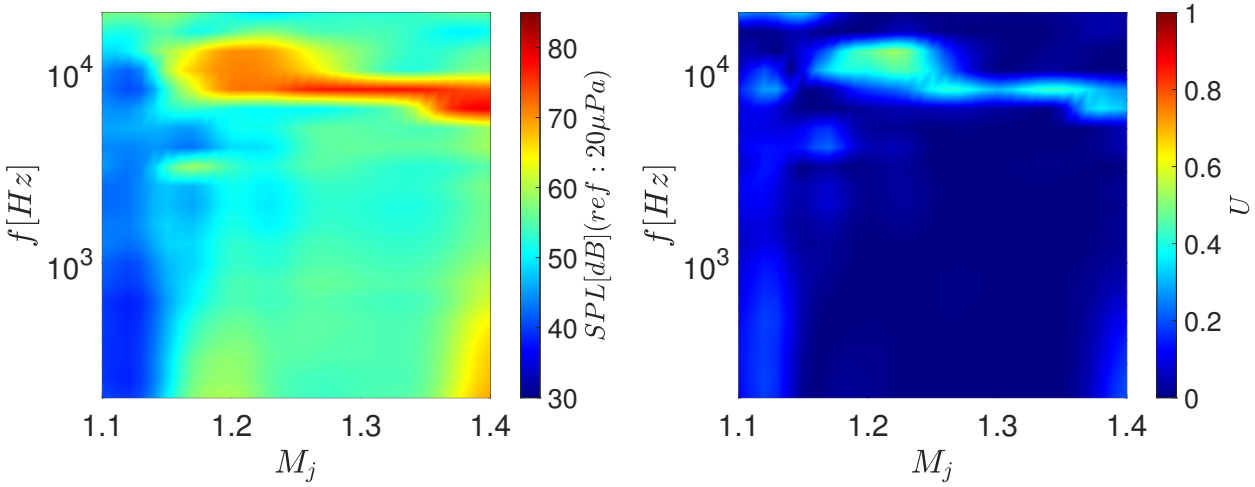


(a) Model response at $h/D = 3.5$ and $x/D = 3.5$

(b) Model uncertainty at $h/D = 3.5$ and $x/D = 3.5$

**Fig. 5 ANN metamodel response and uncertainty at $h/D = 3.5$ and $x/D = 3.5$ for all the Mach numbers between 1.1 and 1.4.**

The ANN model uncertainty map of Fig. 5b shows that the uncertainty values seem to be proportional to the SPL values: this means that the tonal phenomena should be verified by additional experimental data.

Considering another direction of the domain identified by the axial distance: Fig. 6 shows the model response and the uncertainty at $M = 1.33$ and $h/D = 2$ for all the values of $x/D$ between 0 and 18.

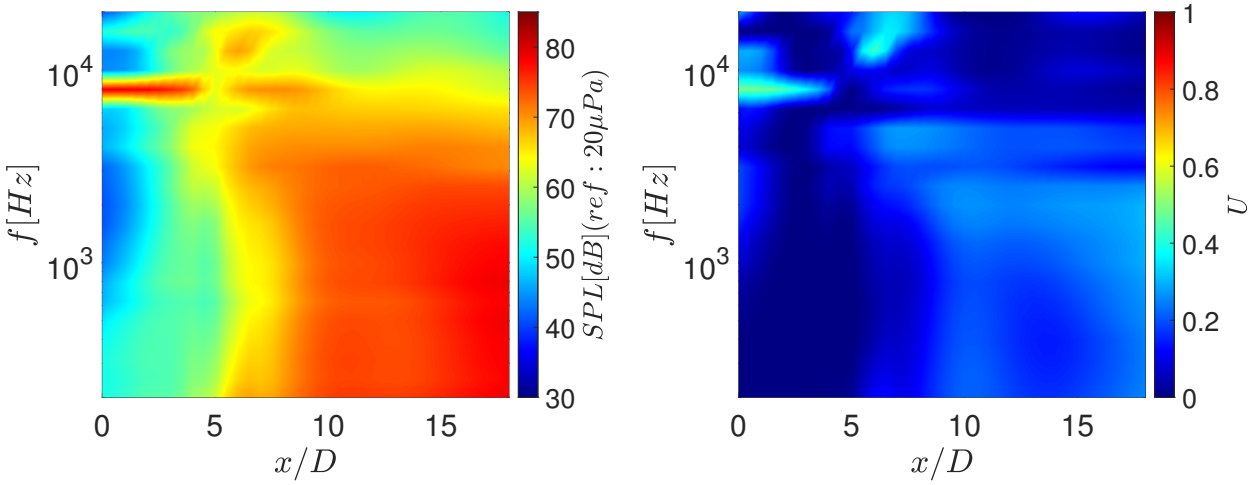


(a) Model response at $M = 1.33$ and $h/D = 2$

(b) Model uncertainty at $M = 1.33$ and $h/D = 2$

**Fig. 6 ANN metamodel response and uncertainty at $M = 1.33$ and $h/D = 2$ for all the values of $x/D$ between 0 and 18.**

As expected, the Screech tone is clearly visible in Fig. 6a at the same frequency of Fig. 7a: its amplitude decreases as $x/D$ increases because of the reduction in intensity of shock–cell sequence. At $x/D \geq 5$ the entire spectrum is dominated by the broadband component and this is ascribed to the jet flow development. The ANN model uncertainty map of Fig. 6b confirms what stated for Fig. 5b: the tonal component's envelope is linked to the maximum uncertainty values, meaning that the high dynamic range of the function should require additional knowledge for enriching the

training set.

The behaviour of the ANN metamodel has been finally explored by varying the last domain direction, the radial location of the microphone array $h/D$, reported in Fig. 7.

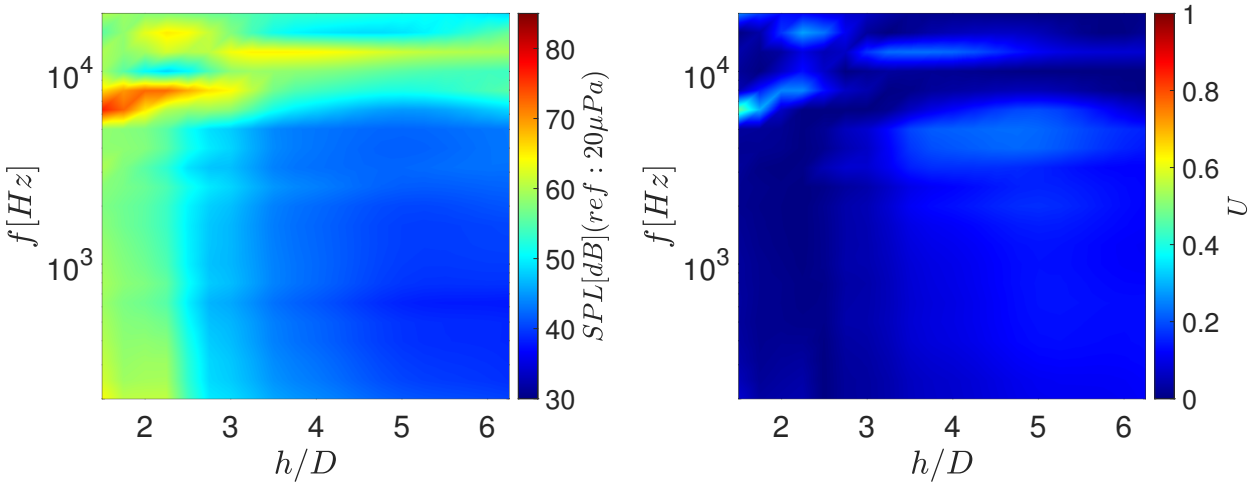


(a) Model response at $M = 1.35$ and $h/D = 2$

(b) Model uncertainty at $M = 1.35$ and $h/D = 2$

**Fig. 7 ANN metamodel response and uncertainty at $M = 1.35$ and $x/D = 3.5$ for all the values of $h/D$ between 1.5 and 6.25.**

As shown in Fig. 7a, the Screech tone remains located at the same frequency and disappears at higher h/D, where the global energy content of the pressure is lower. As for the previous cases also here, the ANN model uncertainty map of Fig. 7b is very low except for some frequency localized zones close to the Screech tone.

The statistics related to the ANN model uncertainty represents the last part of the analysis presented here, and is reported in Fig. 8, in terms of Probability Density Function (PDF) and Cumulative Density Function (CDF).

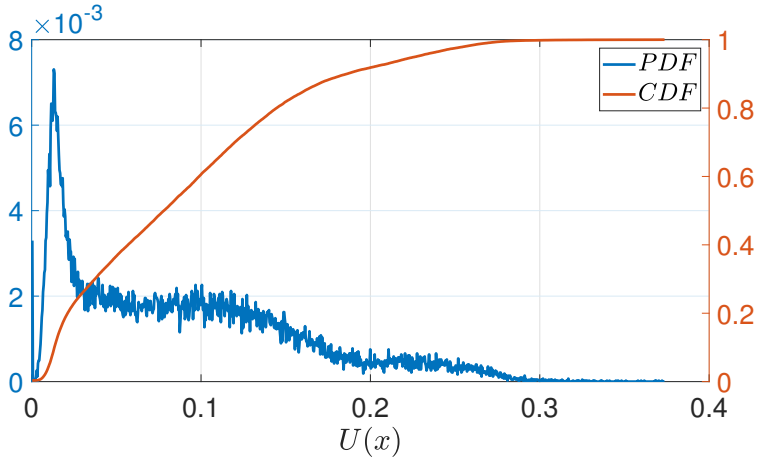


**Fig. 8 Probability Density Function (PDF) and Cumulative Density Function (CDF) related to the ANN model uncertainty.**

The statistical distribution of the uncertainty over the prediction domain is characterised by an expectation $\mu = 0.0893$ with variance $\sigma^2 = 0.0046$. The uncertainty distribution, as shown in Fig. 8, is highly skewed towards low uncertainty values, and there are also several values characterised by zero uncertainty in correspondence with the training points. It is interesting to note that the uncertainty at the 95th percentile is of the same order of magnitude as the training set

target accuracy $\text{RMSE}_{\mathcal{T}}$ and this peculiarity was also found in other analyses carried out by the authors: this property has a paramount relevance in all the problems involving the adaptive sampling, since provides to the designer a criterion to consider the metamodel as final when the true function is not known.

## V. Conclusions

A data–driven nonlinear model aimed at predicting the noise emitted by a cold jet in under–expanded condition has been built and validated. The experimental campaign was conducted at the aeroacoustic facility of the Bristol University: the measurements were carried out for a wide range of under–expanded flow conditions with Mach numbers ranging from 1.1 up to 1.4. The surrogate model is based on artificial neural networks, and a recently–implemented architecture optimization algorithm, coupled with a self–tuning scheme to select the network training parameters, has been used to derive all the relevant parameters. Results show an excellent agreement between the model and the original data, and the predictions related to unknown points are in accordance to the expected physics and the literature. The active algorithm used in this work also provided the uncertainty function, built here based on the spatial correlation between the prediction at the training point and any point within the domain. The uncertainty function can be used to identify the regions of the domain where knowledge of the data should be improved with additional experiments. Within the context of this work, the uncertainty maps revealed that the regions of the domain where additional experiments should be carried out is in correspondence with the Screech tone. Nevertheless, the ANN metamodel has demonstrated to be a viable prediction tool for the jet noise in $1/3$–octave bands.

## Acknowledgements

This work has been supported by the European Union's Horizon 2020 research and innovation program under project ENODISE (Enabling optimized disruptive airframe-propulsion integration concepts) grant agreement No. 860103.

Part of this work was supported by Engineering and Physical Sciences Research Council (EPSRC) Grant No. EP/S000917/1.

## References

[1] Diez, M., Volpi, S., Serani, A., Stern, F., and Campana, E. F., *Simulation-Based Design Optimization by Sequential Multi-criterion Adaptive Sampling and Dynamic Radial Basis Functions*, Springer International Publishing, Cham, 2019, pp. 213–228. doi:10.1007/978-3-319-89988-6_13.

[2] Giunta, A. A., and Watson, L. T., "Using surrogate models and response surfaces in structural optimization with application to crashworthiness design and sheet metal forming," Tech. rep., 1998.

[3] Jones, D. R., "A Taxonomy of Global Optimization Methods Based on Response Surfaces," *Journal of Global Optimization*, Vol. 21, 2001, pp. 345–383. doi:10.1023/A:1012771025575.

[4] Chandrashekarappa, P., and Duvigneau, R., "Radial Basis Functions and Kriging Metamodels for Aerodynamic Optimization," Tech. rep., 2007.

[5] McCulloch, W., and Pitts, W., "A logical calculus of the ideas immanent in nervous activity," *The bulletin of mathematical biophysics*, Vol. 5, 1943, pp. 115–133. doi:10.1007/BF02478259.

[6] Hebb, D., *The Organization of Behaviour*, John Wiley & Sons, Inc., 1949.

[7] Ivakhnenko, A., *Cybernetics and forecasting techniques*, Elsevier Science Ltd, 1967.

[8] Ivakhnenko, A., *Cybernetic predicting devices*, CCM Information Corporation, 1973.

[9] Werbos, P. J., *Beyond Regression: New Tools for Prediction and Analysis in the Behavioral Sciences*, Harvard University, 1975.

[10] Mead, C. A., and Ismail, M., *Analog VLSI Implementation of Neural Systems*, Kluwer Academic Publishers, 1989. doi: 10.1007/978-1-4613-1639-8.

[11] Safran, I., and Shamir, O., "Depth-Width Tradeoffs in Approximating Natural Functions with Neural Networks," *Proceedings of the 34th International Conference on Machine Learning*, Proceedings of Machine Learning Research, Vol. 70, edited by D. Precup and Y. W. Teh, PMLR, International Convention Centre, Sydney, Australia, 2017, pp. 2979–2987.

[12] Shah, M., "Machine Learning Models for Jet Noise Analysis," Master's thesis, The Ohio State University, 2019. Advisor: Gaitonde, Datta.

[13] Brown, C. A., Dowdall, J., Whiteaker, B., and McIntyre, L., *A Machine Learning Approach to Jet-Surface Interaction Noise Modeling*, 2020. doi:10.2514/6.2020-1728, URL https://arc.aiaa.org/doi/abs/10.2514/6.2020-1728.

[14] Centracchio, F., Burghignoli, L., Palma, G., Cioffi, I., and Iemma, U., "Noise shielding surrogate models using dynamic artificial neural networks," *INTER-NOISE and NOISE-CON Congress and Conference Proceedings*, 2021. doi:10.3397/IN-2021-3008.

[15] Burghignoli, L., Rossetti, M., Centracchio, F., Palma, G., and Iemma, U., "Adaptive RBF with hyperparameter optimisation for aeroacoustic applications," *International Journal of Aeroacoustics*, Vol. 21, No. 1-2, 2022, pp. 22–42. doi:10.1177/1475472X221079545.

[16] Camussi, R., Ahmad, M. K., Meloni, S., de Paola, E., and Di Marco, A., "Experimental analysis of an under-expanded jet interacting with a tangential flat plate: Flow visualizations and wall pressure statistics," *Experimental Thermal and Fluid Science*, Vol. 130, 2022, p. 110474. doi:https://doi.org/10.1016/j.expthermflusci.2021.110474, URL https://www.sciencedirect.com/science/article/pii/S0894177721001217.

[17] Huber, J., Fleury, V., Bulté, J., Laurendeau, E., and Sylla, A. A., "Understanding and Reduction of Cruise Jet Noise at Aircraft Level," *International Journal of Aeroacoustics*, Vol. 13, No. 1-2, 2014, pp. 61–84. doi:10.1260/1475-472X.13.1-2.61.

[18] Meloni, S., Camussi, R., Prestianni, M., de Paola, E., and Biondo, F., "An experimental investigation on the unsteady pressure field induced by an installed jet in supersonic flow conditions," *AIAA AVIATION 2021 FORUM*, 2021. doi:10.2514/6.2021-2119.

[19] Harper-Bourne, M., and Fisher, M. J., "The Noise from Shock Waves in Supersonic Jets," *AGARD Conf. Noise Mech*, Vol. 34, 1–13, 1973.

[20] Powell, A., "On the Mechanism of Choked Jet Noise," *Proceedings of the Physical Society. Section B*, Vol. 66, No. 12, 1039–1056, 1953.

[21] Edgington-Mitchell, D., "Aeroacoustic resonance and self-excitation in screeching and impinging supersonic jets – A review," *International Journal of Aeroacoustics*, Vol. 18, No. 2-3, 118-188, 2019.

[22] Norum, T. D., "Screech suppression in supersonic jets," *AIAA Journal*, Vol. 21, No. 2, 1983, pp. 235–240. doi:10.2514/3.8059, URL https://doi.org/10.2514/3.8059.

[23] Tam, C. K. W., "Supersonic Jet Noise," *Annual Review of Fluid Mechanics*, Vol. 27, No. 1, 1995, pp. 17–43. doi:10.1146/annurev.fl.27.010195.000313, URL https://doi.org/10.1146/annurev.fl.27.010195.000313.

[24] Jawahar, H. K., Meloni, S., Camussi, R., and Azarpeyvand, M., *Experimental Investigation on the Jet Noise Sources for Chevron Nozzles in Under-expanded Condition*, 2021, Vol. AIAA AVIATION 2021 FORUM. doi:10.2514/6.2021-2181, URL https://arc.aiaa.org/doi/abs/10.2514/6.2021-2181.

[25] Meloni, S., and Kamliya Jawahar, H., "A Wavelet-Based Time-Frequency Analysis on the Supersonic Jet Noise Features with Chevrons," *Fluids*, Vol. 7, No. 3, 2022. doi:10.3390/fluids7030108, URL https://www.mdpi.com/2311-5521/7/3/108.

[26] Bridges, J., and Brown, C., "Parametric testing of chevrons on single flow hot jets," *10th AIAA/CEAS aeroacoustics conference*, 2004, p. 2824.